JOURNAL OF MATERIALS SCIENCE **35** (2000) 5449–5455

Tensile failure in fiber reinforced ceramic matrix composites

YIH-CHERNG CHIANG
Department of Mechanical Engineering, Chinese Culture University
No. 55, Hua-Kang Rd., Taipei, Taiwan
E-mail: johnycc@gcn.net.tw

The newly derived relationship between the closure traction and the crack opening displacement by the modified shear-lag model is used to investigate the tensile failure behaviors of unidirectional fiber reinforced ceramics. The critical stress for matrix cracking and the critical stress to fracture the fiber are calculated for various crack configurations. Then, the failure of composite initiates as the applied stress exceeds the smaller of the matrix cracking stress and the fiber fracture stress. The differences of results between the present analysis and Marshall and Cox are discussed. Finally, the possible tensile failure modes and the transition conditions between different failure modes are summarized in this paper.

1. Introduction

Under tensile loading in the fiber direction, one of two distinct tensile failures can exhibit for unidirectional fiber reinforced ceramics in which fibers are weakly coupled to the matrix. If the net traction carried by the intact fibers is sufficiently large, the first damage may be in the form of a crack that extends through the matrix without fiber failure. Further loading causes the formation of multiple matrix cracks in the composite. Finally, the composite fails as fibers break. A comprehensive analysis to predict the critical stress to propagate the matrix crack without fiber failure has been given by Chiang, Chou and Wang [1]. On the other hand, if the bridging fibers cannot sustain the additional load originally born by the matrix, the first matrix crack can cause complete failure of the composite. However, the closure traction from the unbroken bridging fibers still can toughen the composite.

Marshall *et al.* (Refs. [2–4]) extended the Marshall Cox and Evans (MCE) [5] model to analyze tensile fracture of unidirectional fiber reinforced ceramics. In these analyses, the fiber strength is assumed to be single-valued and may be weak enough to be broken in the wake of a matrix crack. The implication of the assumption of single-valued fiber strength is that the fiber failure occurs at the crack plane and the fiber failure initiates from the mouth of the fiber-bridged crack. The possibility of fiber failure within the matrix due to the statistical nature of fiber strength cannot be accounted for by the assumption of single-valued fiber strength. In their analyses, the critical applied stress to propagate the matrix crack is determined by the criterion that the stress intensity at the crack tip attains a critical value. On the other hand, the critical applied stress to fracture the fiber is determined by the condition that the fiber in the crack mouth reaches the assumed single-valued fiber strength. The failure of a composite is, then, assumed to initiate as the applied stress exceeds the smaller of these two critical stresses.

Chiang, Chou and Wang [1] have indicated that the closure traction distribution of a fiber-bridged crack cannot be adequately predicted by the MCE model, in which the matrix shear deformation above the slipping region has not been taken into account. However, the tensile failure analyses in Refs. [2–4] is based upon the closure traction predictions. Thus, a more rigorous prediction of closure traction distribution than that of the MCE model is needed to properly analyze the tensile failure behaviors of unidirectional fiber reinforced ceramics. The intention of the present paper is to extend Chiang, Chou and Wang [1] model to reinvestigate the tensile failure behaviors of unidirectional fiber reinforced ceramics. The present results show that very different failure modes are predicted for some crack configurations from the present analysis and the analyses based upon MCE model.

2. Fracture mechanics model

The crack configuration of the present analysis is illustrated in Fig. 1, where a straight crack of length c comprised an initial unbridged length c_0 and a fiber bridging length d. Composite is loaded by a remote uniform stress σ normal to the crack plane. The bridging fiber effect is represented by an equivalent closure traction distribution which is denoted by $T(x)$, while the crack opening displacement is denoted by $2u(x)$. The slipping between the fiber and matrix is over a distance l_s, and the frictional shear stress on the fiber/matrix interface is τ_s.

Now, let the composite be replaced by an effective continuum material, the net closure traction $p(X)$ on the crack surface can be approximated as

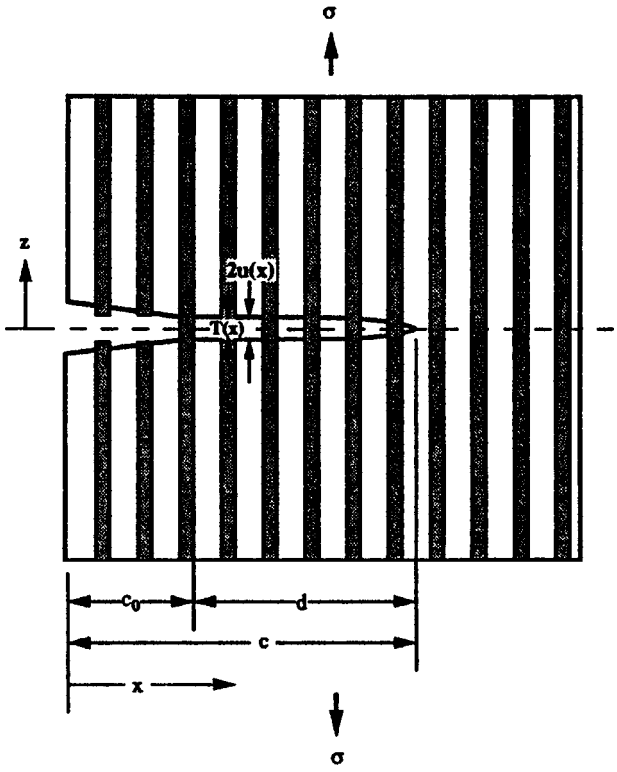

Figure 1 Schematic representation of crack configuration in which a crack length c comprised an initial unbridged crack c_0 and a bridged crack length d.

$$p(X) = 0 \qquad (X < c_0/c) \tag{1a}$$

$$p(X) = V_f T(X) \quad (X \geq c_0/c) \tag{1b}$$

where $X = x/c$ and V_f is the fiber volume fraction.

For an isotropic material with the Young's modulus E_c, and the Poisson's ratio ν_c, the analytical solution of $p(X)$ is related to the entire distribution of crack opening displacement $u(X)$ (Sneddon and Lowengrub [6])

$$u(X) = \frac{4(1-\nu_c^2)c}{\pi E_c} \int_X^1 \frac{s}{\sqrt{s^2 - X^2}} \left\{ \int_0^s \frac{[\sigma - p(t)]\,dt}{\sqrt{s^2 - t^2}} \right\} ds \tag{2}$$

where the composite Young's modulus E_c, can be approximated by the rule-of-mixtures

$$E_c = V_f E_f + V_m E_m \tag{3}$$

The integral Equation 2 contains two unknowns of the crack opening displacement $u(X)$ and the crack closure traction $T(X)$. It is needed to derive one more equation related $u(X)$ and $T(X)$ in order to solve the problem. Chiang, Chou and Wang [1] has adopted a modified shear lag model (see Fig. 2) to derive the $u(X)$-$T(X)$ relationship:

$$u = -\frac{a(V_f E_f - V_m E_m)}{4\tau_s V_m E_m E_f} T^2 + \frac{V_f(\beta\lambda - 1)}{V_m E_m \lambda} T + \frac{aV_m E_m \alpha + aE_f(\sigma + V_f\alpha) - \tau_s E_c \beta^2 \lambda}{aV_m E_m E_f \lambda} \tag{4}$$

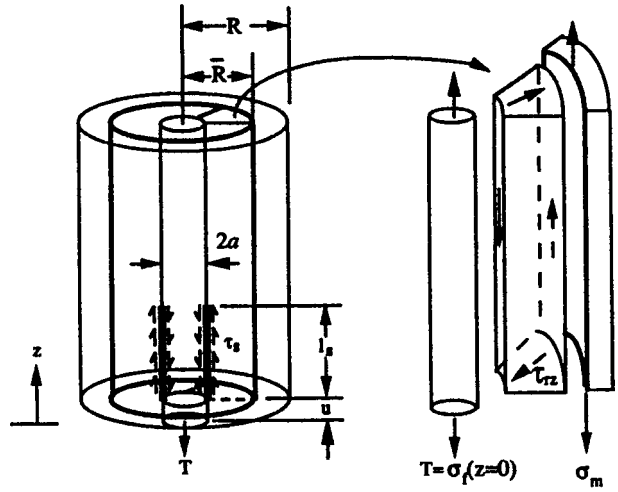

Figure 2 The shear-lag model.

where

$$\alpha = \frac{(V_f T - \sigma)E_f}{2E_c} + \frac{1}{2}\sqrt{\left[\frac{(V_f T - \sigma)E_f}{E_c}\right]^2 + \frac{8\tau_s V_m E_m E_f \ln(\bar{R}/a)}{G_m E_c}}$$

$$\beta = \frac{a}{2\tau_s}\left(\alpha + \frac{E_f \sigma}{E_c}\right)$$

$$\lambda = \frac{\rho}{a}\sqrt{\frac{E_c\alpha + E_f(\sigma - V_f T)}{E_c \alpha}}$$

$$\rho = \sqrt{\frac{2G_m E_c}{V_m E_m E_f \ln(\bar{R}/a)}}$$

In Equation 4, a is the fiber radius and $\bar{R}$ is the equivalent radius of matrix cylinder and its expression is given by Budiansky, Hutchinson and Evans [7]

$$\ln\left(\frac{\bar{R}}{a}\right) = -\frac{2\ln V_f + V_m(3 - V_f)}{4V_m^2} \tag{5}$$

Due to the double integration, Equation 2 is not suitable for numerical process. A simpler equation involving only a single integration was given by McCartney [8]:

$$u(X) = \frac{2(1-\nu_c^2)c\sigma}{\pi E_c} \int_0^1 \left[1 - \frac{V_f T(t)}{\sigma}\right] \times \ln\left|\frac{\sqrt{1-t^2} + \sqrt{1-X^2}}{\sqrt{1-t^2} - \sqrt{1-X^2}}\right| dt \tag{6}$$

Substituting Equation 4 into Equation 6, the nonlinear integral equation becomes

$$T(X) = 0 \quad (X < c_0/c) \tag{7a}$$

$$T^2(X) + AT(X) + B = \gamma\left[\pi\sqrt{1-X^2} - \frac{V_f}{\sigma}\int_0^1 T(t) \times \ln\left|\frac{\sqrt{1-t^2}+\sqrt{1-X^2}}{\sqrt{1-t^2}-\sqrt{1-X^2}}\right| dt\right] \quad (X \geq c_0/c) \tag{7b}$$

Where

$$A = -\frac{4\tau_s V_f E_f(\beta\lambda - 1)}{a\lambda(V_f E_f - V_m E_m)}$$

$$B = -\frac{4\tau_s[aV_f E_f\alpha + aE_f(\sigma + V_f\alpha) - \tau_s E_c\beta^2\lambda]}{a^2\lambda(V_f E_f - V_m E_m)}$$

$$\gamma = -\frac{8(1-\nu_c^2)c\tau_s V_m E_f E_f\sigma}{\pi a(V_f E_f - V_m E_m)}$$

The far-field applied stress, σ, can be regarded as a uniform opening stress acting over the crack surface. Therefore, the net stress on the crack surface is, σ-$p(x)$, and the stress intensity factor K of the composite can be defined as

$$K = 2\sqrt{c/\pi}\int_0^1 \frac{[\sigma - p(X)]\,dX}{\sqrt{1-X^2}} \tag{8}$$

To determine the critical stress for matrix crack propagation, the linear elastic fracture mechanics criterion is adopted, namely, $K = K_{IC}^c$. Gao, Mai and Cotterell [9] assumed that the strain energy release rate of the composite at the crack tip, G_c can be approximated as the work of fracture of the matrix, Γ_m

$$G_c = \frac{1-\nu_c^2}{E_c}K_{IC}^{c^2} = \Gamma_m = \frac{1-\nu_m^2}{E_m}K_{IC}^{m^2} \tag{9}$$

where K_{IC}^c and K_{IC}^m are the critical stress intensity factors of the composite and matrix materials, respectively. If we further discount the Poisson's ratio effect, Equation 9 is reduced to

$$K_{IC}^c = K_{IC}^m\sqrt{E_c/E_m} \tag{10}$$

After obtaining the closure traction $T(X)$ by solving Equation 7, the stress intensity of a fiber-bridged crack is calculated by Equation 8. Then, the critical applied stress, σ^*, and the corresponding closure traction, $T^*(X)$, for a fiber-bridged crack propagating in a composite ($K = K_{IC}^c$) can be determined for various crack configurations.

The highest fiber axial stress is located at the location of $X = c_0/c$ on the crack plane. Therefore, the fiber failure occurs as the fiber stress at $X = c_0/c$ exceeds the assumed single-valued fiber strength S. The critical applied stress, σ #, to initiate the fiber failure is determined by the following condition

$$T^{\#}(c_0/c) = S \tag{11}$$

3. Composite failure modes

The composite system of Nicalon fiber and LAS glass matrix is used for the numerical calculations and its material properties are given in Table I. For the purpose of comparing the present analysis with Marshall and Cox (MC) [3], the normalized stress and crack length defined in their analysis are used

$$\sigma_m = \frac{3}{\sqrt{\pi}}\left(\frac{1.44K_{IC}^{c^2}V_f^2\omega}{\pi}\right)^{1/3} \tag{12a}$$

$$c_m = \left(\frac{\pi K_{IC}^c}{1.44V_f^2\omega}\right)^{2/3} \tag{12b}$$

where $\omega = 8(1-\nu_c^2)\tau_s E_f/a\pi^{1/2}V_m E_m$.

The difference in the predicted crack closure traction distribution between present analysis and MC can be shown in Fig. 3, in which $T^*(X)/\sigma_m$-X curves are plotted for three different c_0 (0, $0.25c_m$, and $0.5c_m$,) at $c = c_m$, and $V_f = 0.5$. The results of MC are also shown in Fig. 3 for the purpose of comparison. For all three cases, the results of $T^*(X)$ by MC approach to 0 at the crack tip. It implies that the fibers at the crack plane do not carry any load as $X \to 1$. This is not a reasonable result because the fibers at the crack plane should carry the load which is originally born by the fibers and matrix in the crack front. From the present analysis, the closure traction, $T^*(X)$, approaches the value of $(E_f/E_c)\sigma$, which is the far-field fiber axial stress, as $X \to 1$.

The other main difference between present analysis and MC is shown in Fig. 4, in which σ^*-c_0/c and $\sigma^{\#}$-c_0/c curves are plotted for the case of $c = c_m$, $V_f = 0.5$ and $SV_f = \sigma_m$. The σ^* value of the present analysis constantly decreases as c_0/c increases. However, the σ^* result of MC is constant from $c_0/c = 0$ to around 0.5 and then decreases still to $c_0/c = 1$. For the $\sigma^{\#}$-c_0/c distribution, the $\sigma^{\#}$ value of present analysis decreases initially and then increases gradually to the value of SV_f. On the other hand, the $\sigma^{\#}$ result of MC decreases slightly and increases dramatically as $c_0/c \to 1$. This is because the MC model predicted zero crack closure traction at the crack tip. This unreasonable result causes the infinite $\sigma^{\#}$ value as $c_0/c \to 1$.

The σ^*-c_0/c and $\sigma^{\#}$-c_0/c curves of different fiber fracture strength are plotted in Fig. 5 for the crack lengths of $c = 0.1c_m$, $0{,}5c_m$, c_m at $V_f = 0.5$. The matrix cracking stress σ^* always decreases as c_0/c increases for various crack length. However, the $\sigma^{\#}$-c_0/c

TABLE I Properties of SiC/LAS composite

	SiC[!]/LAS[@]
E_f	200 Gpa
E_m	85 Gpa
ν_m	0.25
a	8 μm
K_m	2.0 Mpa-$\sqrt{m}$
τ_s	1-2 MPa

[!]Nicalon
[@]Data from Refs. [10] and [11].

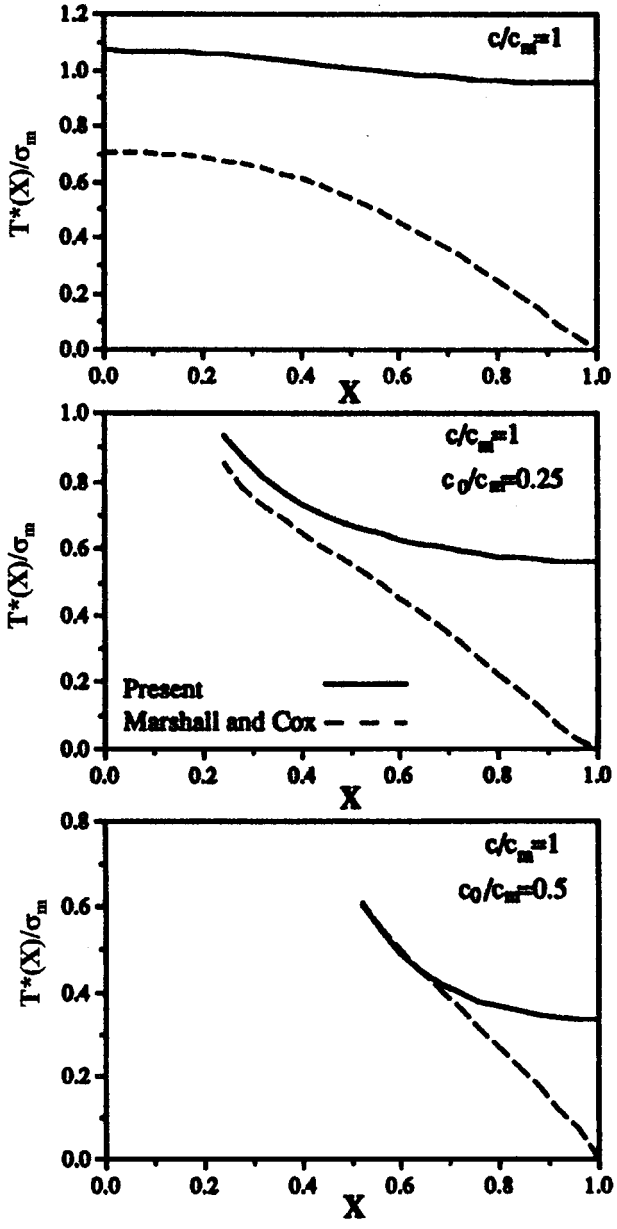

Figure 3 $T^*(X)/\sigma_m$-X distribution.

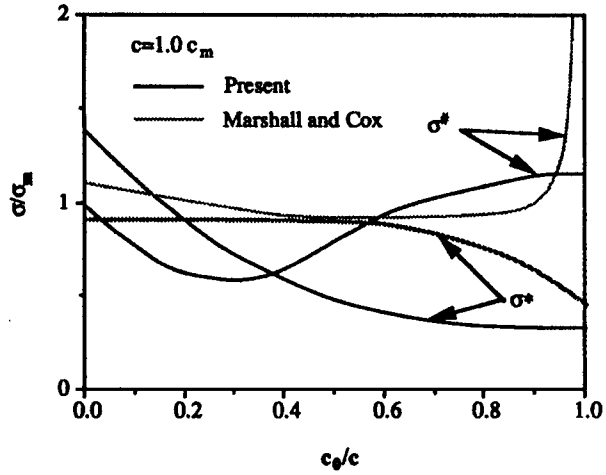

Figure 4 Comparison of σ^*-c_0/c relationships between present analysis and MC.

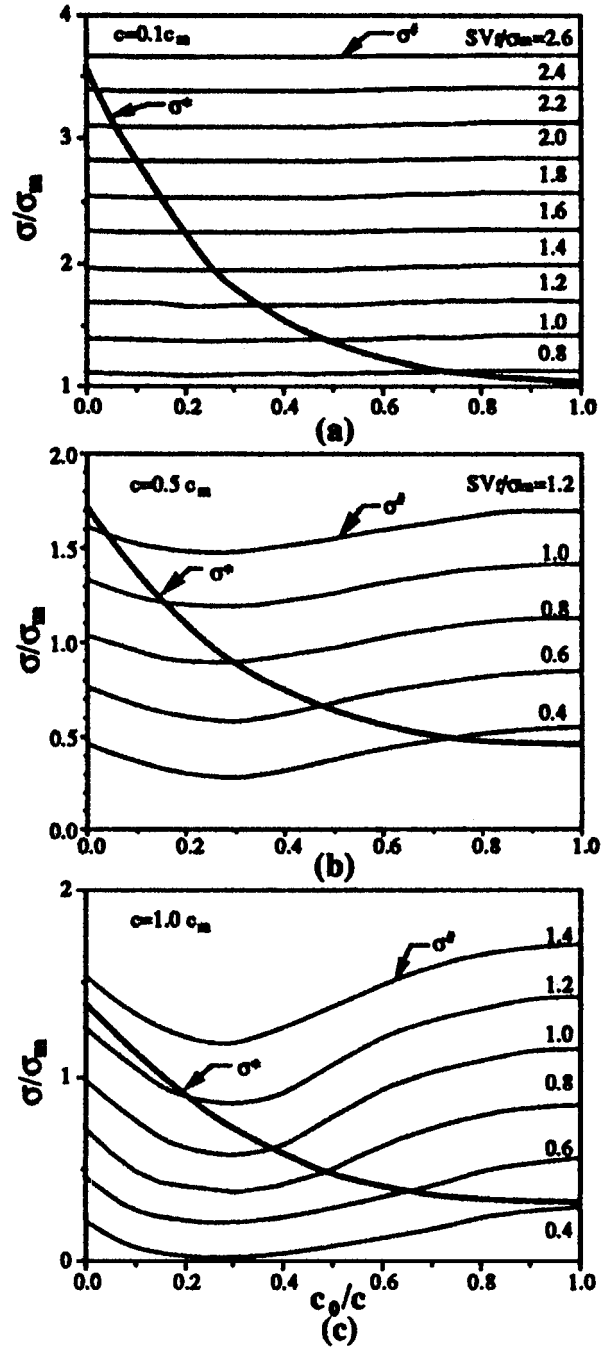

Figure 5 The σ^*-c_0/c curves and $\sigma^{\#}$-c_0/c curves at different fiber strengths for various crack lengths.

distribution depends on the crack length c. For the case of $c = 0.1c_m$, the fiber fracture stresses $\sigma^{\#}$ are almost independent of c_0/c and are equivalent to the value of SV_f, as shown in Fig. 5a. As the crack length c increases, the fiber fracture stress $\sigma^{\#}$ decreases initially and then increases gradually to the value of SV_f, as shown in Fig. 5b and c.

When the fiber strength is not sufficiently large, the fiber fracture may accompany the matrix cracking depending on the fiber strength and the crack configuration. Generally, the failure of a composite initiates when the applied stress exceeds the smaller stress of the stress for matrix cracking and the stress to fracture the fiber. Under the constant applied load, the subsequent failure process may involve the combination of stable or unstable matrix cracking and gradual or catastrophic fiber failure. The various failure modes that depend on the microstructures of composite and the crack configuration are summarized in Table II and the details are discussed in the following.

TABLE II Summary of the failure modes

Failure mode 1	This failure mode causes the multiple matrix cracking and a large nonlinear strain occurs before the complete failure of the composite.
Failure mode 2	Unstable fiber failure accompanies with matrix cracking after Some unstable fiber failure. This causes catastrophic composite failure at the applied stress $\sigma^{\#}$.
Failure mode 3	Unstable fiber failure occurs initially and is followed by stable fiber failure and finally accompanies with matrix cracking.
Failure mode 4	Fibers continue to fail within the matrix after the complete fracture of fibers through the crack length.
Failure mode 5	Stable matrix cracking occurs first and is followed by unstable fiber failure and finally accompanies with unstable matrix cracking.
Failure mode 6	Stable matrix cracking and followed by unstable fiber failure.
Failure mode 7	Stable matrix cracking followed by unstable fiber failure and finally unstable fiber failure and matrix cracking occur simultaneously.

3.1. Initially fully-bridged cracks

The matrix cracking stress, σ^*, and the fiber fracture stress, $\sigma^{\#}$, as a function of normalized crack length, c/c_m, are plotted in Fig. 6 for the initially fully-bridged cracks. Physically, the crack length should be larger than a fiber diameter for a fiber-bridged crack. Therefore, the smallest crack for the calculation is chosen as one fiber diameter ($\sim$0.05 c_m). If the net fiber strength is sufficiently large (i.e. $SV_f/\sigma_m > 2.6$), the entire $\sigma^{\#}$ curve is higher than σ^* curve. The matrix crack propagates through the composite completely without causing fiber failure. Further increasing of the applied load is needed to fracture fibers. This failure mode causes the multiple matrix cracking and a large nonlinear stress-strain curve occurs before the complete failure of composite (Failure mode 1 in Table II).

When the normalized net fiber strength SV_f/σ_m, is between 1 and 2.6, σ^* curve will intercept $\sigma^{\#}$ curve at the crack length c^*. Two different failure modes may occur depending on the crack length c. For the initial crack length c larger than c^*, the matrix cracking stress is smaller than the fiber fracture stress as the crack propagates. The composite failure mode is the same as the Failure mode 1 in Table II. For the initial crack length c smaller than c^*, unstable fiber failure occurs first and then, subsequently, accompanies with unstable matrix cracking. This causes catastrophic composite failure at the applied stress $\sigma^{\#}$ (Failure mode 2 in Table II). This failure mode differs from the MC model in which the matrix cracking occurs first.

When the normalized net fiber strength SV_f/σ_m is smaller than 1, the fiber failure always occurs first. The subsequent events depend on the fiber strength and crack configuration. If the fiber fracture curve can intercept the matrix cracking curve, there are two different failure modes. The first case is shown in Fig. 7a, in which the unstable fiber failure occurs first and then the unstable matrix cracking accompanies fiber fracture. This failure mode is the same as Failure mode 2 in Table II. The second case is illustrated in Fig. 7b, in which the unstable fiber failure occurs initially and then the stable fiber failure follows and finally the unstable matrix cracking accompanies fiber fracture (Failure mode 3 in Table II). On the other hand, if the net fiber strength is so weak that $\sigma^{\#}$-c_0/c curve cannot intercept σ^*-c_0/c curve, fibers continue to fail within the matrix after the complete fracture of fibers through the crack length (Failure mode 4 in Table II). This failure mode cannot occur by the analysis of MC

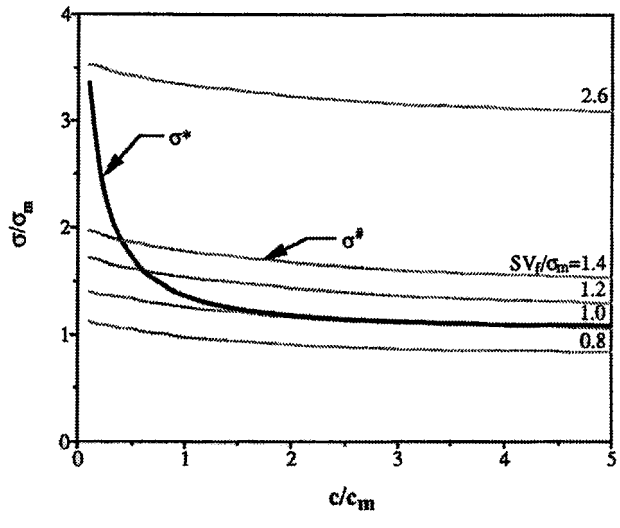

Figure 6 The matrix cracking stress, σ^*, and the fiber fracture stress, $\sigma^{\#}$, as a function of normalized crack length, c/cm for the initially fully-bridged cracks.

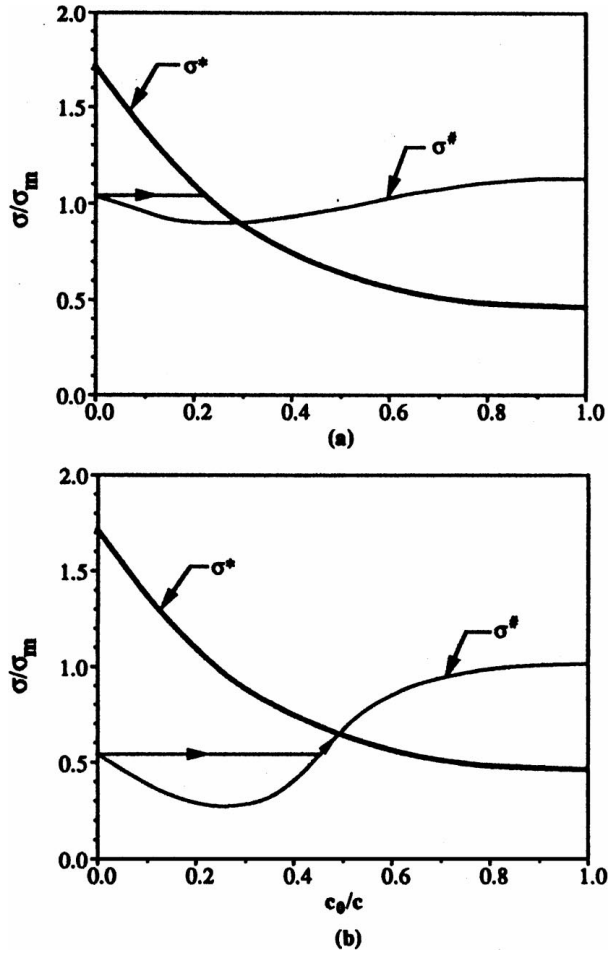

Figure 7 Some cases of σ^*-c_0/c and $\sigma^{\#}$-c_0/c relationships.

because the fiber fracture stress, $\sigma^{\#}$, becomes infinite as $c_0/c \to 1$. It implies that the fiber failure cannot occur for the crack configurations with small fiber-bridged length.

3.2. Initially unbridged cracks

The general features of curves σ^* and $\sigma^{\#}$ for initially unbridged cracks are plotted in Fig. 8 as a function of d/c_m. The failure modes of composites depend on the fiber strength and crack configuration. For the small initial crack length c (see Fig. 8a), four different failure modes could occur. As the fiber strength is smaller than S1, the failure mechanism is described by Failure mode 4 in Table II. When the fiber strength is located between S1 and S2, the failure mode is the same as Failure mode 2 in Table II. For the fiber strength between S2 and S3, the stable matrix cracking occurs first and then is followed by unstable fiber failure and finally accompanies unstable matrix cracking (Failure mode 5 in Table II). As the fiber strength is larger than S3, the multiple matrix cracking described by Failure mode 1 in Table II occurs.

For the larger initial crack length c (Fig. 8b), the failure mechanisms for the fiber strength smaller than S1 and larger than S3 are same as those of small initial crack length c, just described above. As the fiber strength between S1 and S2, the stable matrix cracking is followed by unstable fiber failure (Failure mode 6 in Table II). As the fiber strength between S2 and S3, the stable matrix cracking is followed by unstable fiber failure and finally unstable fiber failure and matrix cracking occur simultaneously (Failure mode 7 in Table II).

3.3. Partially bridged cracks

Compared to initially unbridged cracks, the representation of a partially bridged zone reduces the stress intensity at the crack tip. The failure modes of cracks with partially bridged zone depend on the initial crack length c_0. If the initial crack length c_0 is smaller than the intersection of σ^* and $\sigma^{\#}$ curves (see Fig. 8), the composite exhibits the similar failure behavior as the composite with a unbridged crack. On the other hand, if the initial crack length c_0 is larger than the intersection of σ^* and $\sigma^{\#}$ curves, the failure modes of the composite are similar to those of initially fully-bridged cracks.

4. Discussion and conclusions

1. The crack opening displacement-crack closure traction (u-T) relationship, which accounts the matrix shear deformation above the slipping length and satisfies the far-field boundary condition, has been used to analyze the tensile failure of unidirectional fiber reinforced ceramics. Results show that the newly derived u-T relationship casts a profound influence on the failure mode predictions, especially for the crack configurations of small fiber bridging length or alternative the small cracks.

2. The difference of predicted closure traction between the present analysis and the MC model can be shown in Fig. 9, where $T^*(0)$ is plotted as a function of crack length for the case of fully-bridged cracks. The

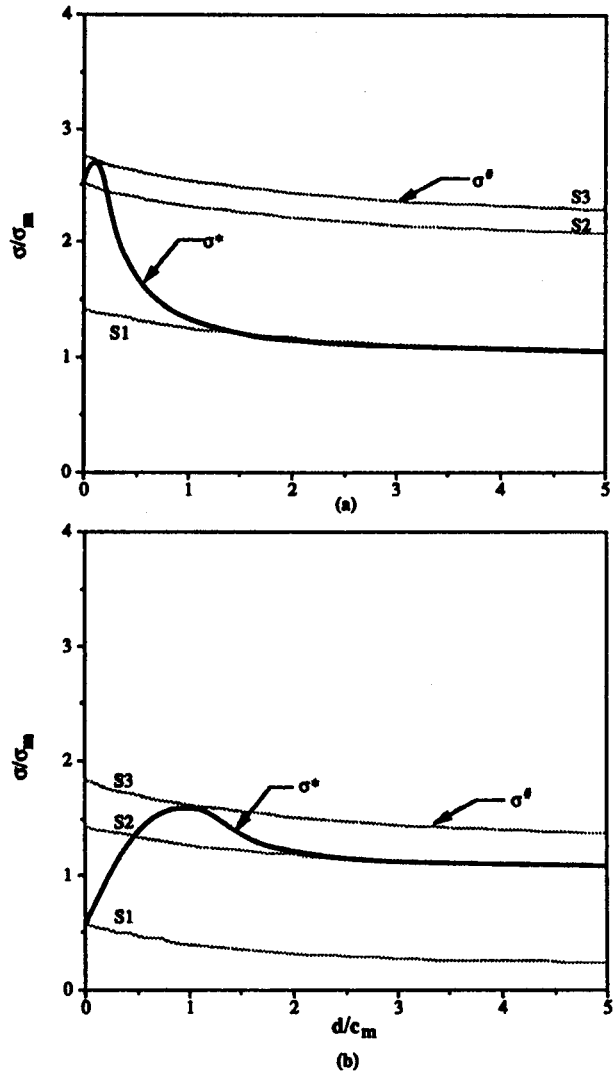

Figure 8 Some cases of σ^*-d/c_m and $\sigma^{\#}$-d/c_m relationships.

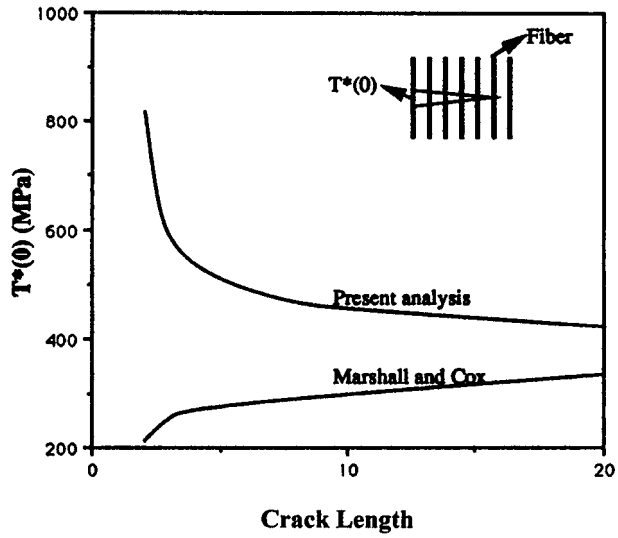

Figure 9 Comparison of $T^*(0)$-c/D results between the present analysis and MC, where D is fiber diameter.

results diverge between two analyses as the crack length approaches zero and they become closer as the crack length becomes longer. The diverged closure traction prediction as $c \to 0$ between two analyses causes the different failure mode predictions, as demonstrated in this paper.

3. The major difference in the failure mode predictions can be shown by the σ^*-c_0/c and $\sigma^\#$-c_0/c relationships between two analyses, as illustrated in Fig. 5. From the Marshall and Cox analysis, the failure of the composite always initiates from matrix cracking for the crack configurations of $c_0/c \to 1$. This is because the closure traction in their analysis vanishes at the crack tip (see Fig. 3). This is not physically realistic, as discussed above. On the other hand, from the present analysis the failure of the composite could initiate from the fracture of fibers for the crack configurations of $c_0/c \to 1$ if the net fiber strength is below a certain value.

4. The tensile failure behaviors influenced by the fiber strength, crack configurations and material properties have been analyzed in the present paper. The possible tensile failure modes and the transition conditions between different failure modes are summarized in Table II.

References

1. Y. C. CHIANG, A. S. D. WANG and T. W. CHOU, *J. Mech. Phys. Solids* **41**(7) (1993) 1137.
2. D. B. MARSHALL and A. G. EVANS, "Fracture Mechanics of Ceramics," Vol. 7 (Plenum, New York 1986) p. 1.
3. D. B. MARSHALL and B. N. COX, *Acta Metall.* **35**(11) (1987) 2607.
4. D. B. MARSHALL and A. G. EVANS, *ibid.* **37** (1989) 2567.
5. D. B. MARSHALL, B. N. COX and A. G. EVANS, *ibid.* **33**(11) (1985) 2013.
6. I. N. SNEDDON and M. LOWENGRUB, "Crack Problem in the Classical Theory of Elasticity" (Wiley, New York 1969).
7. B. BUDIANSKY, J. W. HUTCHINSON and A. G. EVANS, *J. Mech. Phys. Solids* **34**(2) (1986) 167.
8. L. N. MCCARTNEY, *Proc. R. Soc.* **A409** (1987) 329.
9. Y. C. GAO, Y. W. MAI and B. COTTERELL, *J. of Applied Mathematics and Physics (ZAMP)* **39**(7) (1988) 550.
10. M. W. BARSOUM, P. KANGUTKAR and A. S. D. WANG, *Composite Science and Technology* **44** (1992) 271.
11. D. C. PHILLIPS, "Fibre Reinforced Ceramics," Handbook of Composites, Vol. 4-Fabrication of Composites, edited by A. Kelly and S. T. Mileiko (Elsevier Science Publisher, 1983).

Received 21 May 1999
and accepted 20 March 2000